Colloids and Surfaces B: Biointerfaces 183 (2019) 110387

Contents lists available at ScienceDirect

Colloids and Surfaces B: Biointerfaces

journal homepage: www.elsevier.com/locate/colsurfb

Development of theranostic active-targeting boron-containing gold nanoparticles for boron neutron capture therapy (BNCT)

Chun-Yi Wu[a,b,**], Jia-Jia Lin[a], Wen-Yi Chang[c], Cheng-Ying Hsieh[d], Chin-Ching Wu[e], Hong-Sen Chen[f], Hung-Ju Hsu[f], An-Suei Yang[f], Ming-Hua Hsu[d], Wei-Ying Kuo[f,*]

[a] Department of Biomedical Imaging and Radiological Science, China Medical University, Taichung, Taiwan
[b] Master Program for Biomedical Engineering, China Medical University, Taichung, Taiwan
[c] Department of Nuclear Medicine, Taipei Veterans General Hospital, Taipei, Taiwan
[d] Department of Chemistry, National Changhua University of Education, Changhua, Taiwan
[e] Department of Public Health, China Medical University, Taichung, Taiwan
[f] Genomics Research Center, Academia Sinica, Taipei, Taiwan

ARTICLE INFO

Keywords:
Boron neutron capture therapy
Gold nanoparticle-boron cage assemblies
Anti-HER2 antibody

ABSTRACT

Successful boron neutron capture therapy (BNCT) requires sufficient and specific delivery of boron atoms to malignant cells. Gold nanoparticles (AuNPs) have been used as a useful delivery system for selectively releasing cytotoxic payloads in the tumor. However, studies demonstrating the *in vivo* distribution or pharmacokinetics of boron-containing AuNPs via noninvasive imaging are lacking. This study aims to develop theranostic AuNP-boron cage assemblies (B-AuNPs) and evaluate its feasibility for BNCT. The commercial citrate-coated AuNPs were subjected to PEGylation, azide addition, and carborane modification on the surface. To further arm the AuNPs, we conjugated anti-HER2 antibody (61 IgG) with boron-containing PEGylated AuNPs to form 61-B-AuNPs. The diameter and radiolabeling efficiency of boron-containing AuNPs were determined by dynamic light scattering (DLS) and radio thin-layer chromatography (radio TLC), respectively. Noninvasive single-photon emission computed tomography (SPECT)/computed tomography (CT) imaging was performed to determine the pharmacokinetics of radioiodinated AuNPs in N87 gastric cancer xenografts, and the content of boron in tumor and muscle was assessed by inductively coupled plasma mass spectrometry (ICP-MS). After the 3-step modification, the diameter of B-AuNPs increased by ~25 nm, and antibody conjugation did not affect the diameter of AuNPs. Radioactive iodine (I-123) was introduced in AuNPs by Click chemistry under copper catalysis. The radiolabeling efficiency of ^{123}I-B-AuNPs and ^{123}I-61-B-AuNPs was approximately 60 ± 5%. After purification, the radiochemical purity (RCP) of these NPs was greater than 90%. MicroSPECT/CT imaging showed that the tumor-to-muscle (*T/M*) ratio of ^{123}I-B-AuNP-injected mice reached 1.91 ± 0.17 at 12 h post-injection, while that of ^{123}I-61-B-AuNP-injected mice was 12.02 ± 0.94. However, the increased uptake of AuNPs by the thyroid was observed at 36 h after the administration of ^{123}I-61-B-AuNPs, indicating antibody-mediated phagocytosis. The *T/M* ratio, assessed by ICP-MS, of B-AuNP- and 61-B-AuNP-injected mice was 4.91 ± 2.75 and 41.05 ± 11.15, respectively. We successfully developed detectable HER2-targeting boron-containing AuNPs with high RCP and an acceptable yield. Noninvasive imaging could be a valuable tool for the noninvasive determination of the pharmacokinetics of AuNPs and measurement of boron concentration in the tumor.

1. Introduction

Boron neutron capture therapy (BNCT) is a binary treatment approach. Neither neutron beam nor boron drugs alone can cause tissue damage. However, when a boron atom is specifically retained in the tumor, it could capture a neutron under neutron irradiation and undergo fission reactions to produce Lithium-7 (Li-7) and α-particles, which would release energy within a limited distance, generally, less than a diameter of a cell. Therefore, how to deliver sufficient boron atoms into tumor lesions is the key success factor in BNCT.

Nowadays, only two boron-containing compounds are routinely used clinically: L-4-dihydroxyborylphenylalanine (BPA) and sodium

* Corresponding author at: Genomics Research Center, Academia Sinica, 128 Academia Road, Section 2, Nankang, Taipei 11529, Taiwan.
** Corresponding author at: Department of Biomedical Imaging and Radiological Science, China Medical University, 91 Hsueh-Shih Rd., Taichung 40402, Taiwan.
E-mail addresses: cywu@mail.cmu.edu.tw (C.-Y. Wu), d40020005@gm.ym.edu.tw (W.-Y. Kuo).

https://doi.org/10.1016/j.colsurfb.2019.110387
Received 26 April 2019; Received in revised form 8 July 2019; Accepted 23 July 2019
Available online 01 August 2019
0927-7765/ © 2019 Elsevier B.V. All rights reserved.

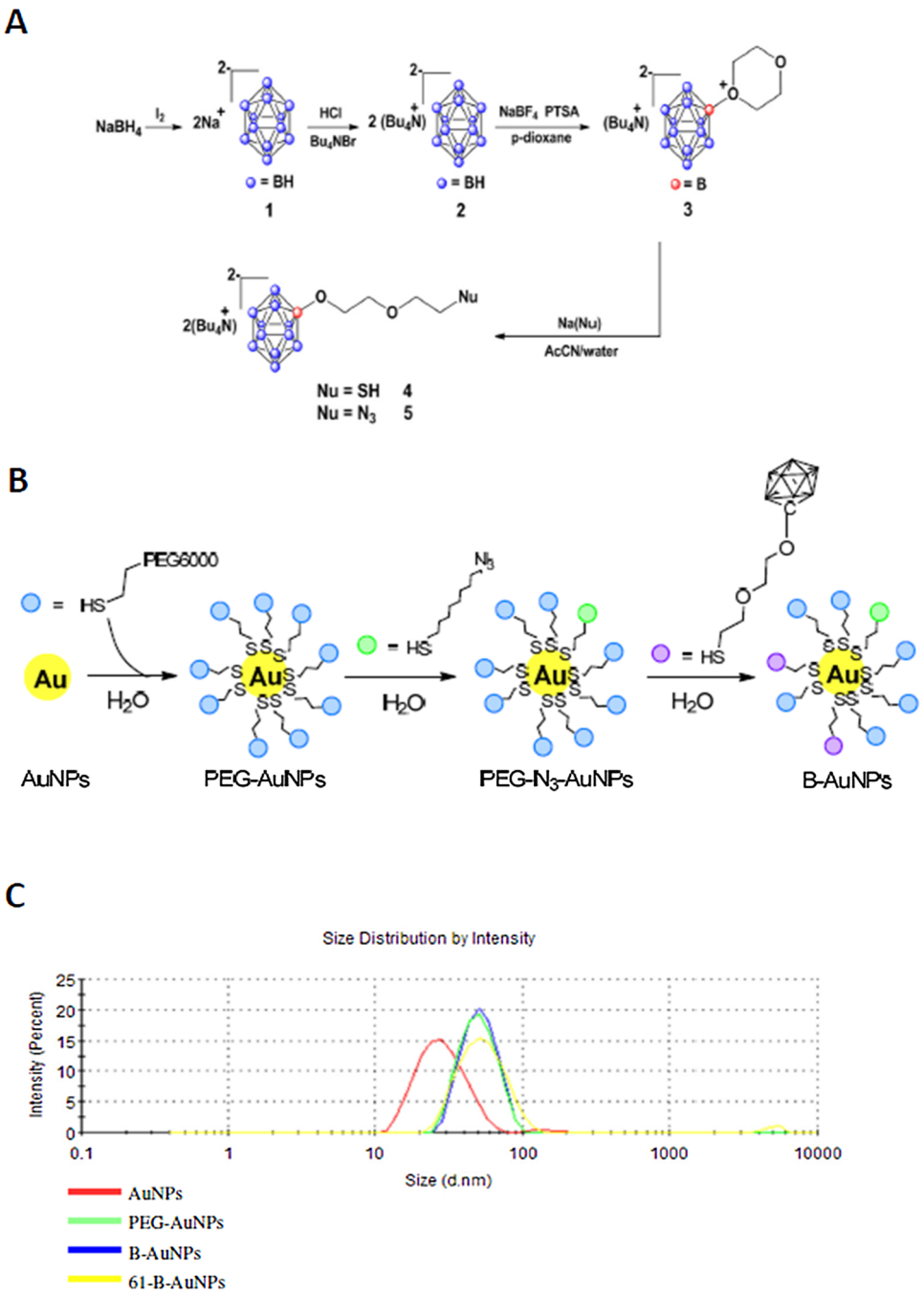

Fig. 1. (A) The synthetic scheme of boron cage-SH (4). (B) The synthetic scheme of B-AuNPs. (C) DLS graphs of AuNPs (red), PEGylated AuNPs (green), B-AuNPs (blue), and 61-B-AuNPs (yellow) (For interpretation of the references to colour in this figure legend, the reader is referred to the web version of this article).

borocaptate (BSH). The boron content of BSH is much higher than that of BPA, but its major disadvantage is the lack of specificity. Several groups have used drug delivery systems, such as liposomes, micelles, carbon nanotubes or dendrimers, to increase the accumulation of boron compounds in the tumor, thus enhancing the therapeutic effect of BNCT [1]. The enhanced permeability and retention effect is based on the relatively leaky blood vessel structure of tumors, which allows nanoparticles (NPs) ranging in size from 100 to 200 nm to easily pass through tumor blood vessel wall and stay in the tumor rather than in healthy tissue.

Gold NPs (AuNPs) present some advantages for BNCT when compared with other drug carriers as follows. First, AuNPs of uniform and small particle size can be easily developed, which would potentially diminish their accumulation in the liver [2]. Second, the Au core (Au-197) may be activated during neutron irradiation to form Au-198 [3], which would release β-particles, ultimately killing the tumor cells. The combination of α- and β-particles may elevate the response to BNCT. Third, Kubota et al. reported that AuNPs induce strong oxidative stress within the cells, causing autophagic cell death [2]. Thus, AuNPs might be a more powerful weapon when armed with boron atoms for BNCT.

Studies on boron-containing compounds and AuNPs as boron carriers have been summarized by Hosmane et al. [4–6]. Among the synthetic approach to modify the surface of AuNPs, “Click” chemistry is a good choice due to the high efficiency. Djeda et al. synthesized carborane-appended large dendrimers containing 81 o-carborane clusters by using Click synthesis [7]. Liang et al. first discovered the characteristics of the combination of AuNPs and o-carborane-rich clusters for BNCT [8]. Li et al. also reported a simple approach to modifying the

membrane of AuNPs with polyethylene glycol (PEG) and BSH via Click chemistry under copper catalysis [9]. Ciani et al. linked PEG with BSH through Click chemistry and then attached these blocks onto AuNPs using Au-sulfur (S) linkages to prepare boron-containing AuNPs [10]. However, studies on using noninvasive imaging technique to determine the *in vivo* distribution or pharmacokinetics of active-targeting PEGylated AuNP-carborane assemblies are still limited to date.

Although the small size of AuNPs could decrease non-specific binding in the liver, the level of retention of NPs within tumors needs further improvement. Human epidermal receptor-2 (HER2) is a well-known therapeutic target and has been overexpressed on the membrane of various types of cancer cells. To further enhance the tumor uptake of AuNPs, Kubota et al. synthesized trastuzumab-functionalized AuNPs and demonstrated their potent antitumor effects against HER2-positive and trastuzumab-resistant subcutaneous xenografts [2]. Recently, Chen et al. integrated anti-HER2 single-chain variable fragments (ScFv), a fluorescent dye, PEG moieties, and chelate for radiolabeling within silica NPs of < 10 nm diameter. The results revealed a progressively increased BT474 xenograft uptake of trastuzumab-conjugated NPs over time [11]. Our previous studies demonstrated that a self-developed anti-HER2 antibody, named 61 IgG, exhibited superior HER2-targeting ability and could induce receptor-mediated endocytosis [12], which may be beneficial for boron atom accumulation in the cytoplasm of tumor cells rather than in the interstitial space. Therefore, in this study, we prepared ^{123}I-labeled anti-HER2 AuNP-boron cage assemblies and evaluated its feasibility as a theranostic agent for patient selection prior to BNCT.

2. Materials and methods

2.1. Materials

Citrate-coated AuNPs (20 nm diameter) was purchased from Sigma-Aldrich Co. (St. Louis, USA). Sephadex G-50 Fine was obtained from GE Healthcare (Illinois, USA). N-succinimidyl S-acetylthioacetate (SATA) was purchased from Pierce Chemical Co. (Illinois, USA). All other chemicals were purchased from Sigma-Aldrich Co. (St. Louis, USA). The instant thin-layer chromatography plate coated with silica gel (ITLC-SG) was obtained from Varian Inc. Radiolabeled sodium iodide ($Na^{123}I$) was obtained from the Institute of Nuclear Energy Research (Taoyuan, Taiwan). The anti-HER2 antibody (61 IgG) was kindly provided by Prof. An-Suei Yang (Academia Sinica, Taiwan). Boron cage-SH (BC-EG-SH; Fig. 1A) was a gift from Prof. Ming-Hua Hsu. Cell culture dishes, flasks, and plasticware were purchased from Corning Inc. (New York, USA). Fetal bovine serum (FBS) and culture medium were purchased from Thermo Fisher Scientific (Massachusetts, USA).

2.2. The preparation of boron-containing gold nanoparticles

Boron-containing AuNPs were prepared from commercial citrate-coated AuNPs. The surface modification of AuNPs is shown in Fig. 1B. PEG6000 (0.72 mg, 0.12 μmol) was added to a vial containing citrate-coated AuNP solution (6.54×10^{11} particles), and the reaction mixture was reacted at room temperature (RT) in dark for 1 h. After the removal of unconjugated PEG6000 by centrifugation at 3,220 × *g* for 20 min at 4 °C, dodecanethiol azide (55 ng, 0.24 nmol) was dissolved in acetone (10 μL) and added to the solution of PEGylated AuNPs. The reaction mixture was stirred at RT for 1 h and then centrifuged at 3,220 × *g* for 20 min at 4 °C to remove unconjugated azide. Finally, the addition of self-synthesized boron cage-SH (28.29 mg, 37.72 μmol) was applied to give the crude product, which was then centrifuged (3220 × *g*, 20 min, 4 °C) to obtain the final product in the form of a pellet. The diameter of boron-containing AuNPs was determined by dynamic light scattering (DLS; Malvern #ZS90).

2.3. Synthesis of propargyl-PEG2000-OMe

To a stirred suspension of 60% sodium hydride (144 mg, 6 mmole) in mineral oil in dry DMF (10 mL), PEG2000-OMe (4 g, 2 mmole) was added at RT and stirred for 30 min. Propargyl bromide (420 μL, 3.9 mmole) was added drop-wise, and the reaction mixture was heated to 80 °C for 24 h. After quenching with 3 mL of water under vigorous stirring, the solvent was evaporated under reduced pressure. The resulting slurry was diluted with 30 mL of dichloromethane and washed with water. The organic phase was dried over magnesium sulfate, filtered and concentrated under reduced pressure to a final volume of approximately 10 mL. This solution was poured into cold 200 mL of diethylether and cooled to −5 °C for 30 min, until the solution was completely crystallized. The precipitate was filtered and discarded, and washed thoroughly with cold diethyether. This purification process was repeated one more time. Ultimately, 3 g (1.5 mmole, 75%) of compound **7** was obtained as a slightly brown solid. ^{1}H-NMR (400 MHz, $CDCl_3$): δ 4.0 (d, J = 1.8, 2 H), 3.62-3.36 (m, 191 H), 3.28 (s, 3 H), 2.42 (s, 1 H)

2.4. Preparation of thiol-modified 61 IgG

SATA-modified 61 IgG was prepared as described previously [13]. Briefly, SATA (15.4 μg, 66.7 nmol) was added to a vial containing 61 IgG (1 mg, 6.67 nmol) and incubated at RT for 1 h. The crude product was then loaded onto a Sephadex G50 column for purification. The resulting SATA-modified 61 IgG was then treated with 200 μL of 0.5 M hydroxylamine at RT for 2 h, to produce the crude product. The desired product, 61 IgG-SH, was obtained after purification using the Sephadex G50 column.

2.5. Radioiodination of AuNPs

Copper (II) chloride (1.34 mg, 0.01 mmol) dissolved in acetonitrile (400 μL) and triethanolamine (2 μL) was added into the vial containing alkynylated PEG2000 (2 mg, 10 μmole) at r.t. for a 5-min reaction as catalyst solution. B-AuNPs were mixed with 5 μL of freshly prepared catalyst solution, and then the $Na^{123}I$ solution (1~2 mCi) was added into this vial immediately for a 15-min reaction at r.t to give crude ^{123}I-B-AuNPs. The radiolabeling efficiency of ^{123}I-B-AuNPs was accessed by radio thin layer chromatography (instant thin-layer chromatography plate coated with silica gel, ITLC-SG, Merck) with H_2O as the mobile phase. The crude product was purified by centrifugation (3220 g, 20 min, 4 °C) for removal of free radioiodine to give ^{123}I-B-AuNPs with high radiochemical purity (> 90%).

The protocol for antibody conjugation to ^{123}I-B-AuNPs was basically based on the method published by Kumar et al. [14]. The 61 IgG-SH (100 μg/mL) was loaded into ^{123}I-B-AuNPs suspension and then reacted at r.t. for 1 h. The mixture was centrifuged (2500 g, 20 min, 4 °C) and the resulting pellet was washed twice with distilled water to remove unbound 61 IgG to give ^{123}I-61-B-AuNPs.

2.6. The stability of ^{123}I-labeled AuNPs

The radiolabeled AuNPs were incubated in either normal saline at RT or FBS at 37 °C for 0, 1, 2, 4, 8, 12, 24, or 36 h. To determine the percentage of intact radioactive nanoparticles at these time points, the stability of radiolabeled AuNPs was analyzed by radio TLC.

2.7. Cell cultures and xenograft inoculation

The N87 human gastric cancer cells were grown in RPMI 1640 medium supplemented with 10% FBS at 37 °C in a humidified atmosphere containing 5% CO_2. To conduct xenograft inoculation, approximately 1×10^6 N87 cells in 100 μL of Matrigel:serum-free medium mixture (1:1, v/v) were subcutaneously implanted into the

right flank of 6-week-old male NOD/SCID mouse. When the tumor size reached 150 ± 50 mm^3, the mice were selected for further experiments.

2.8. In vitro cellular uptake and internalization assays

Approximately 1×10^6 cells were seeded in a 6-well plate and cultured in culture medium containing 10% FBS (3 mL) for at least 24 h. The culture medium was replaced with serum-free medium containing radiolabeled NPs (3 mL, 0.074 MBq/mL). At 4, 12, 24, and 36 h post-incubation, the medium was aspirated, and cells were washed twice with PBS (0.5 mL) to remove unbound ^{123}I. The medium and washing buffer were collected in a counting vial. Cells were treated with 0.5 mL of 0.25% trypsin for 5 min to facilitated their detachment from the plate. The cells were then collected and resuspended in 1.5 mL of serum-containing medium to neutralize the activity of trypsin. The number of cells in the cell suspension was measured using a hemocytometer for normalization. The cellular uptake of radiolabeled NPs was expressed as the percentage of administered dose accumulated in one million cells (%AD/10^6 cells).

The internalization assay was performed as described previously [12]. Cells collected from the cellular uptake experiment at each time points were resuspended in a solution (1 mL) containing 200 mM sodium acetate and 500 mM sodium chloride (pH = 2.5) and incubated at 4 °C for 5 min to remove the cell-surface bound ^{123}I from the cells. After centrifugation at 8000 × *g* for 10 min, the cells were washed with PBS twice. Both the supernatant and washing buffer were collected into a vial, and the cell pellets were added to another counting vial to measure the radioactivity. Internalization was expressed as a percentage of initially bound radioactivity.

2.9. MicroSPECT/CT imaging of radioiodinated AuNPs

The microSPECT/CT images were acquired using the imaging modality at Cheng Gung Memorial Hospital, Taiwan (nanoSPECT/CT, Mediso). Static imaging was carried out for approximately 30 min at 12 and 36 h after the administration of 37 MBq of either ^{123}I-61-B-AuNPs or ^{123}I-B-AuNPs. Quantified tissue uptake was calculated as the average number of pixels within the tumor and selected muscle. The tumor-to-muscle (*T/M*) ratio was used to normalize differences among individuals and to determine the specific tumor uptake.

2.10. Assessment of radioactivity accumulation in tissues

The xenografted mice were sacrificed at 12 h post-injection of 3.7 MBq of either ^{123}I-61-B-AuNPs or ^{123}I-B-AuNPs (n ≥ 5 mice in each group). Samples of blood and different tissues (heart, lung, liver, stomach, small intestine, large intestine, pancreas, spleen, muscle, kidney, bone, bone marrow, thyroid, and tumor) were harvested, cleaned, and weighed, and the level of radioactivity retained in these samples was measured using a gamma counter (Cobra II Auto-Gamma Counter, Perkin-Elmer Inc., USA). Tissue uptake was expressed as a percentage of the injected dose per gram of sample weight (%ID/g).

2.11. Assessment of boron content in tumor and muscle

Boron concentration in tumor and muscle was determined by inductively coupled plasma mass spectrometry (ICP-MS). Mice injected with either ^{123}I-61-B-AuNPs or ^{123}I-B-AuNPs (n = 3 in each group) were sacrificed immediately after microSPECT/CT imaging at 36 hpi. Parts of the tumor and muscle were excised, weighed, homogenized, and subjected to ICP-MS analysis using ELAN DRC ROMAN II ICP mass spectrometer (Perkin-Elmer). Boron concentration was expressed as μg/g tissue.

2.12. Statistical analysis

All values were expressed as mean ± standard derivation. The Student's *t*-test was used for the comparison between groups. Differences with p-value < 0.05 were regarded as statistically significant.

3. Results

3.1. Gold nanoparticles surface modification

The diameter of commercial citrate-coated AuNPs was approximately 23.93 ± 10.22 nm and increased by 25 nm (49.73 ± 19.19 nm) after modification with PEG6000 (Fig. 1C). However, the diameter of NPs showed no significant change after modification with dodecanethiol azide (57.02 ± 14.16 nm) and boron cage-SH (57.59 ± 13.90 nm) because the size of these two reagents does not compare to that of PEG6000. The size of active-targeting AuNPs (61-B-AuNPs; 54.48 ± 14.72 nm) was similar to that of B-AuNPs (Fig. 1C). Li et al. and Kubota et al. also found that the addition of PEG increased the diameter of AuNPs by approximately 10–15 nm [2,9]; however, Kubota et al. demonstrated that further modification of trastuzumab on PEGylated AuNPs would result in slightly decreased size [2]. Additionally, the centrifugation speed and time exerted a significant effect on the average size of these NPs. For example, combination of greater centrifugation speed (4000 × *g*) and longer time (30 min) increased the yield of collected NPs; however, it also resulted in the increased number of larger-sized NPs because of aggregation (Fig. S2), which may cause liver trapping *in vivo*. The large-sized aggregates were not noticed at each step.

3.2. The preparation of radioiodinated AuNPs

The radioactive isotope of iodine (^{123}I) was introduced in AuNPs by Click chemistry under copper catalysis (Fig. 2A), with a labeling efficiency of 60 ± 5% (Fig. 2B). After purification, the RCP of ^{123}I-B-AuNPs was greater than 90% (Fig. 2C). The RCP of ^{123}I-61-B-AuNPs was slightly higher than that of ^{123}I-B-AuNPs because ^{123}I-61-B-AuNPs was experienced an extra round of centrifugation to remove unconjugated 61 IgG (Fig. 2D). The radiochemical yield (RCY) of ^{123}I-B-AuNPs and ^{123}I-61-B-AuNPs was 56.33 ± 6.56% and 25.88 ± 4.32%, respectively. To avoid aggregation, the samples were subjected to low-speed centrifugation, causing the loss of radioactivity, as all the AuNPs could not be separated from the solution. In the stability tests, the percentage of intact ^{123}I-B-AuNPs and ^{123}I-61-B-AuNPs was greater than 90% after an 8-h incubation in normal saline at RT but was relatively lower when incubated in FBS at 37 °C (Fig. 3). However, the RCP of ^{123}I-B-AuNPs and ^{123}I-61-B-AuNPs at 36 h after incubation in FBS was 77.8 ± 1.8% and 72.6 ± 2.1%, respectively. No difference was detected between the RCP of these two radioiodinated AuNPs at all time points.

3.3. Assessment of in vitro cellular uptake and internalization percentage

The cellular uptake of ^{123}I-61-B-AuNPs and ^{123}I-trastuzumab-B-AuNPs (expressed as %AD/10^6 cells) increased with time, reaching a maximum accumulation of 19.66 ± 2.71 and 23.31 ± 4.84, respectively, at 36 h post-incubation. However, the accumulation of ^{123}I-B-AuNPs remained low throughout the 36-h study period. These results indicate that surface modification with HER2-targeting antibodies enhances the specific uptake of AuNPs (Table 1).

The percentage of initially bound activity of NPs in internalization assays is shown in Table 1. Although ^{123}I-trastuzumab-B-AuNPs showed the highest cellular uptake among these three NPs at each time point, the internalized fraction of these NPs declined with time. At 36 h post-incubation, only 8.57 ± 0.89% of bound activity was retained in cells. On the contrary, the percentage of radioactivity of ^{123}I-61-B-AuNPs

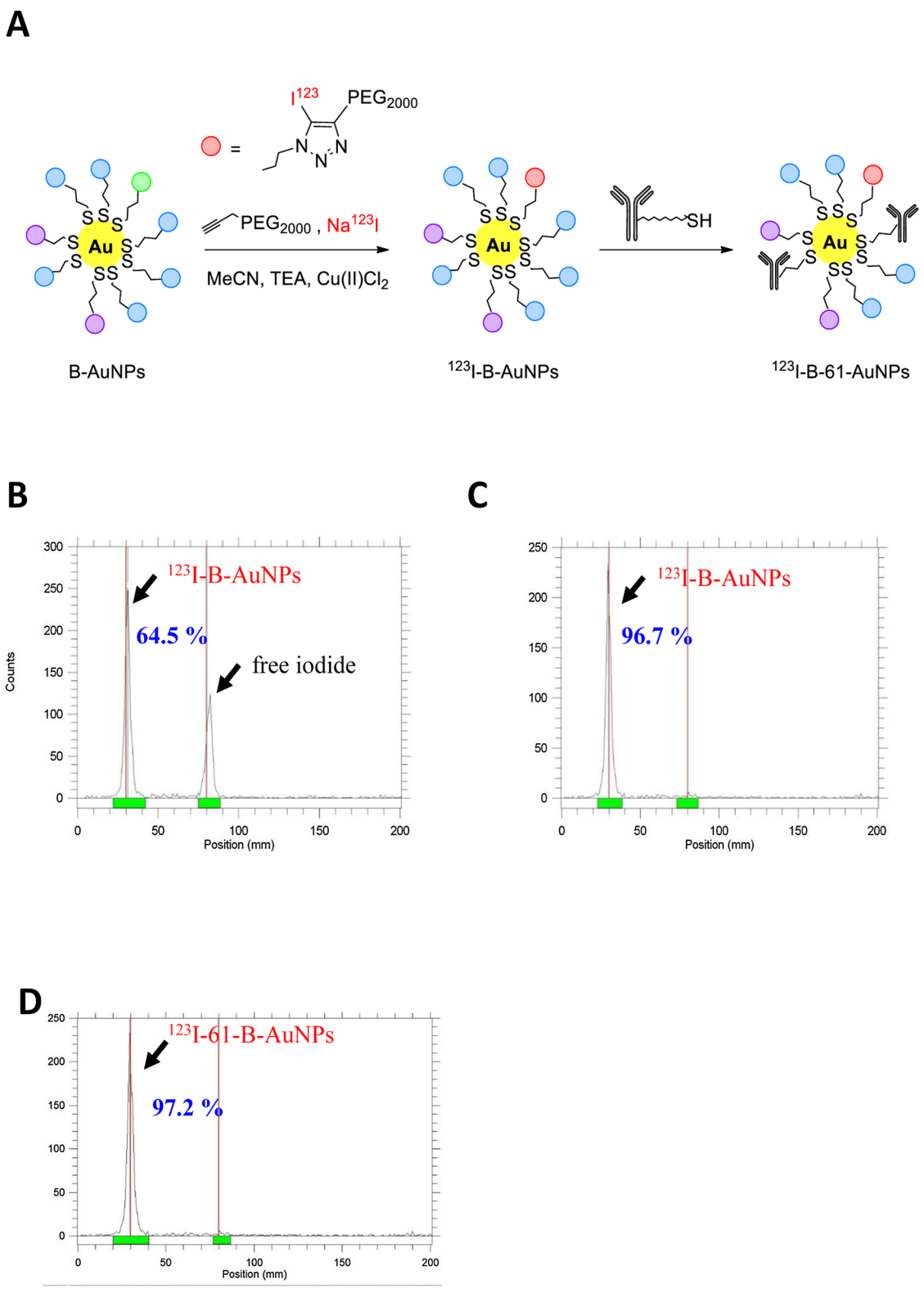

Fig. 2. (A) The synthetic scheme of ^{123}I-B-AuNPs and ^{123}I-61-B-AuNPs. RadioTLC graphs of ^{123}I-B-AuNPs (B) before purification, (C) after purification, and (D) ^{123}I-61-B-AuNPs. The Rf values of ^{123}I-B-AuNPs, ^{123}I-61-B-AuNPs, and unlabeled radioactive iodine are 0, 0, and 1, respectively.

internalized in cells increased from 10.53 ± 1.21% at 12 h to 15.40 ± 1.72% at 36 h post-incubation. The radioactivity of ^{123}I-B-AuNPs inside the cells was similar to the background, suggesting zero internalization.

3.4. Animal SPECT/CT imaging

The results of microSPECT/CT imaging showed that the more apparent accumulation of ^{123}I-61-B-AuNPs in the tumor occurred at 12 hpi, suggesting that the anti-HER2 antibody acts as effective targeting component against HER2 expression in the tumor membrane

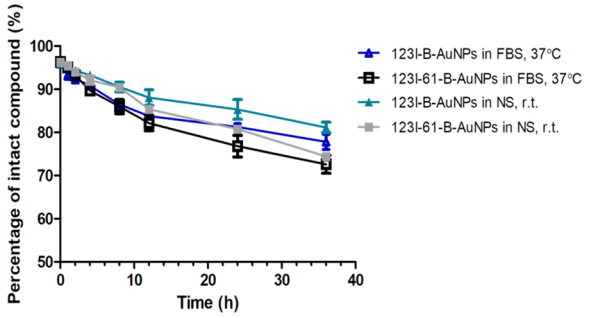

Fig. 3. *In vitro* stability of ^{123}I-B-AuNPs and ^{123}I-61-B-AuNPs in either normal saline at r.t. or in fetal bovine serum at 37 °C.

(Fig. 4). The tumor uptake of AuNPs in mice injected with ^{123}I-61-B-AuNPs was 48.32 ± 3.11%ID/mL at 12 hpi, which was higher than that of AuNPs in mice injected with ^{123}I-B-AuNPs (7.43 ± 0.28%ID/mL). The *T/M* ratio of ^{123}I-B-AuNPs and ^{123}I-61-B-AuNPs was 1.91 ± 0.17 and 12.02 ± 0.94 at 12 hpi, respectively. Most of the ^{123}I-B-AuNPs were retained in the liver and spleen, and only a few ^{123}I-B-AuNPs were detected in N87 xenograft, as both of these organs are rich in the reticuloendothelial system (RES). A similar result was observed in a mouse model with an orthotopic SASVO3 human tongue squamous carcinoma xenograft (Fig. S1). No apparent radioactivity retention was detected in the thyroid at 12 and 36 hpi, indicating the *in vivo* stability of ^{123}I-B-AuNPs. The off-target accumulation of 61 IgG-modified AuNPs in the liver and other normal organs was lower than that of ^{123}I-B-AuNPs. However, the *T/M* ratio of mice injected with ^{123}I-61-B-AuNPs decreased from 12.02 ± 0.94 at 12 hpi to 1.09 ± 0.14 at 36 hpi, and a significant increase in radioactivity accumulation was observed in the thyroid at 36 hpi. By contrast, the *T/M* ratio of the ^{123}I-B-AuNP-administered group increased only slightly to 4.50 ± 0.16 at 36 hpi, possibly because of antibody-mediated phagocytosis.

3.5. Assessment of radioactivity accumulation in tissues

Except the tumor, blood, liver, and spleen at 12 hpi, tissue samples showed no significant difference in the AuNP uptake between the mice injected with ^{123}I-B-AuNPs and those injected with ^{123}I-61-B-AuNPs (Fig. 5). In the tumor of mice receiving ^{123}I-B-AuNPs and ^{123}I-61-B-AuNPs, the uptake of AuNPs was 1.61 ± 0.16 and 9.09 ± 0.21%ID/g, respectively. The *T/M* ratio of ^{123}I-61-B-AuNP-injected mice was 7.42 ± 0.61, which was also higher than that of ^{123}I-B-AuNP-injected mice (1.34 ± 0.09). The tumor uptake of ^{123}I-61-B-AuNPs was the highest among all excised normal organs, including liver and spleen. However, the tumor to blood ratio of ^{123}I-B-AuNP-injected mice was only 0.57 ± 0.07, and the liver showed the highest uptake among these organs, suggesting a severe off-target effect. Although micro-SPECT images showed relatively low thyroid accumulation, it was 2-fold higher than that in the muscle in both groups. Generally, the results obtained from biodistribution studies were in accordance with those derived from microSPECT/CT imaging.

3.6. Assessment of boron content in tumor and muscle

The boron concentration of all samples was determined by ICP-MS. The intratumoral boron concentration of ^{123}I-61-B-AuNP- and ^{123}I-B-AuNP-injected mice was 217.1 ± 47.1 and 74.5 ± 6.0 μg/g sample, respectively, at 36 hpi, while the *T/M* ratio was 23.1 ± 5.9 and 4.9 ± 2.8, respectively (Table 2). A strong positive correlation was observed between the *T/M* ratio acquired from biodistribution studies at 12 hpi and that obtained from ICP-MS at 36 hpi (R^2 = 0.85; Fig. 6).

4. Discussion

To date, no materials containing AuNPs have been approved by the US Food and Drug Administration for clinical use. Several studies suggest that the dose-limiting toxicity of AuNPs, particularly to RES-rich and excretory organs, is the key factor to advance beyond pre-clinical trails. However, considering that Au compounds were applied as therapeutics for patients with progressive rheumatoid disease over three decades ago, the safety of AuNPs may be not a concern [15].

The AuNPs are conjugated with an antibody to avoid their non-specific accumulation in RES-rich organs. The development of antibody-based therapy for the treatment of tumor has progressively increased in recent decades. Trastuzumab, a commercial monoclonal antibody, targets HER2 overexpressed on the membrane of human breast and gastric cancer cells and obstructs the proliferation of signal transduction caused by HER2 dimerization. Trastuzumab also induces antibody-dependent cellular cytotoxicity, thus inhibiting tumor growth. Jiang et al. indicated that 40–50 nm was the optimal size of trastuzumab-AuNPs; these AuNPs significantly enhanced receptor-mediated internalization, thus down-regulating the expression of pMAPK and increasing caspase-9 and caspase-3 cleavage, with greater cell death than that caused by trastuzumab alone [16]. However, these findings were based on *in vitro* experiments; therefore, the effect of *in vivo* delivery efficiency on internalization was unknown [16]. Kubota et al. also demonstrated that trastuzumab-modified AuNPs, with a diameter of 85.39 ± 0.68 nm, exhibited strong *in vitro* cytotoxicity toward both trastuzumab-sensitive and trastuzumab-resistant gastric cancer cells [2]. The tumor did not receive sufficient AuNPs after intravenous injection due to intense liver uptake, while intratumoral injection of 5×10^9 Herceptin-AuNPs three times a week showed significant therapeutic efficacy [2]. Therefore, in this study, we used small-sized AuNPs (~20 nm) as a starting material for surface modifications to reduce non-specific accumulation after systemic delivery.

In our previous work, we demonstrated that 61 IgG induces an apparent internalization within tumors and causes a lower liver uptake compared with trastuzumab *in vivo*. At a relatively low dose, 61 IgG-drug conjugates exhibit a significant tumor-killing effect compared with trastuzumab in N87 human gastric cancer xenograft [12,17]. The different epitope of HER2 recognized by 61 IgG may account for its higher internalization rate [18]. In this study, the cellular uptake and internalization assays indicated the highest percentage of initial radioactivity of ^{123}I-61-B-AuNPs in N87 cells (Table 1), suggesting the potential of ^{123}I-61-B-AuNPs as a carrier for *in vivo* drug delivery. Further

Table 1
Cellular uptake and internalization of ^{123}I-B-AuNPs, ^{123}I-61-B-AuNPs, and ^{123}I-trastuzumab-B-AuNPs in N87 cells.

^{123}I-B-AuNPs			^{123}I-61-B-AuNPs		^{123}I-trastuzmab-B-AuNPs	
	Uptake[a]	Internalization[b]	Uptake	Internalization	Uptake	Internalization
4 h	1.23 ± 0.12	–	5.62 ± 0.27	–	6.69 ± 0.20	–
12 h	1.17 ± 0.03	0.56 ± 0.06	10.77 ± 0.43	10.53 ± 1.21	13.62 ± 1.12	12.58 ± 1.50
24 h	1.14 ± 0.07	0.55 ± 0.09	14.60 ± 1.36	14.69 ± 1.44	19.40 ± 1.42	10.48 ± 1.01
36 h	0.97 ± 0.05	0.42 ± 0.16	19.66 ± 2.71	15.40 ± 1.72	23.31 ± 4.84	8.57 ± 0.89

[a] Cellular Uptake (%uptake/10^6 cells).
[b] Internalization (%).

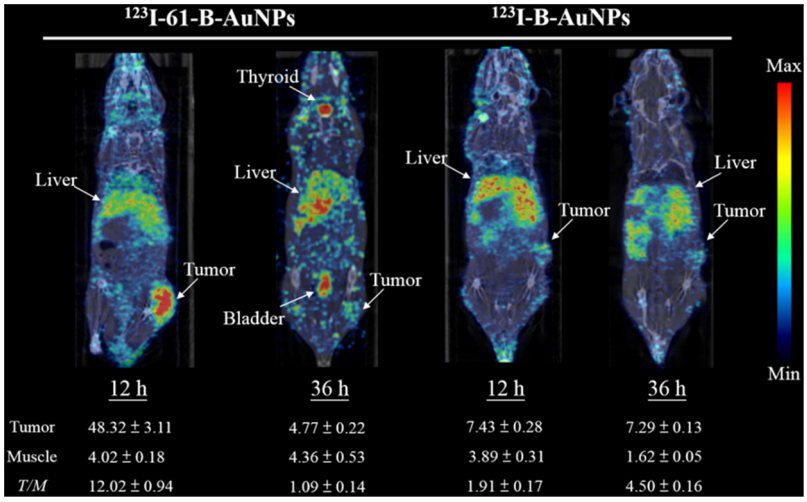

Fig. 4. MicroSPECT/CT images of N87 xenograft-bearing mice intravenously injected with 37 MBq of ^{123}I-B-AuNPs and ^{123}I-61-B-AuNPs at 12 and 36 h p.i.

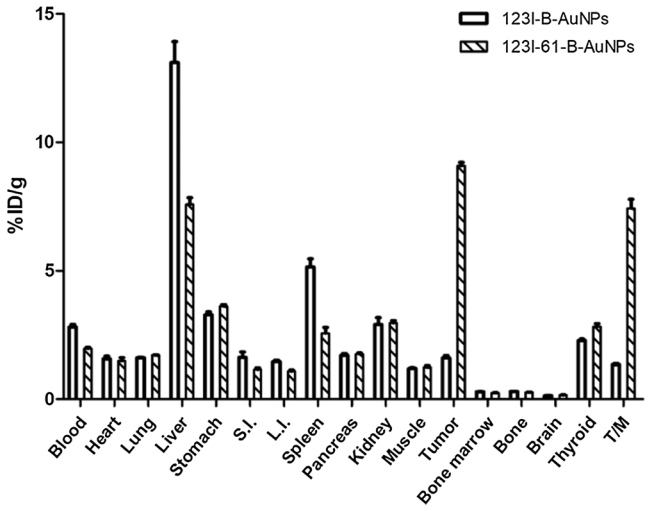

Fig. 5. Radioactivity distribution of ^{123}I-B-AuNPs and ^{123}I-61-B-AuNPs in N87 xenograft-bearing mice at 12 h after intravenous injection.

Table 2
The boron content in tumor and muscle determined by ICP-MS.

B content	^{123}I-B-AuNPs	^{123}I-61-B-AuNPs
Injected dose (μg)	1788.3 ± 245.1	1419.2 ± 153.3
Encapsulation efficiency	35.8 ± 5.6	28.4 ± 4.3
Tumor (μg/g)	74.5 ± 6.0	217.1 ± 47.1
Muscle (μg/g)	20.7 ± 12.8	9.4 ± 1.3
Tumor uptake (%)	4.2 ± 0.7	15.3 ± 3.7
T/M	4.9 ± 2.8	23.1 ± 5.9

examination of the distribution of ^{123}I-B-AuNPs revealed that most of the radioactivity was retained in the liver, while only a small amount of ^{123}I-B-AuNPs was observed in either N87 cells or SASVO3 tumors (Fig. 4, Fig. S1). A significant uptake of ^{123}I-61-B-AuNPs in N87 xenograft was observed at 12 h after systemic injection via the tail vein (Fig. 4). Regarding the similarity of the diameters of ^{123}I-B-AuNPs and ^{123}I-61-B-AuNPs, the key factor for enhancing the *in vitro* and *in vivo* tumor uptake should be the modification of AuNPs with 61-IgG. High accumulation of ^{123}I in the thyroid was observed at 36 h post ^{123}I-61-B-AuNP administration, suggesting that ^{123}I-61-B-AuNPs were internalized and transported to lysosomes, wherein under acidic conditions, ^{123}I-61-B-AuNPs were degraded and free iodine was released.

Theoretically, BNCT can eradicate cancer cells, depending on the

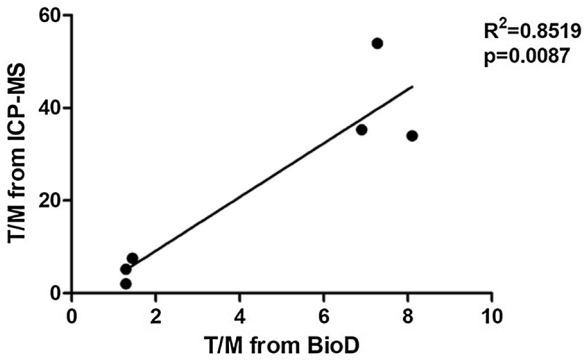

Fig. 6. Correlation between the T/M obtained from biodistribution studies and that derived from boron content determined by ICP-MS (R2 = 0.8519, $p < 0.05$).

specific and sufficient accumulation of boron atoms in malignant cells rather than normal cells. Generally, 20 μg ^{10}B/g tumor uptake and at least 3:1 tumor to background ratio lead to a good treatment outcome. Considering the low boron content of BPA (0.416%), the used boron atoms should be enriched in ^{10}B atoms (> 99%) and continuous infusion should be generally used to achieve sufficient B-10 concentration in blood. Although the boron encapsulation efficiency of ^{123}I-B-AuNPs and ^{123}I-61-B-AuNPs was only 35.75 ± 3.69% and 28.38 ± 4.86%, respectively, which is not as high as the AuNPs used to carry boron atoms (previously published, [2]), the tumor uptake of ^{123}I-61-B-AuNPs, determined by the ICP-MS assay, reached 217.1 ± 47.1 μg B/g tumor at 36 hpi. Given that the natural abundance of ^{10}B in boron atom is 19.8%, the ^{10}B content of the tumor at 36 hpi was approximately 73.91 ± 9.32 μg ^{10}B/g tumor, which is much higher than 20 μg ^{10}B/g tumor. These findings suggest that we can directly use natural boron atoms rather than enriched ^{10}B to prepare these kinds of NPs for clinical use, implying that the cost of therapy would be much lower. Additionally, continuous infusion could be replaced by a single bolus injection, which is more convenient for patients. The *T/M* ratio of ^{123}I-B-AuNPs and ^{123}I-61-B-AuNPs, assessed by ICP-MS, was 4.91 ± 2.75 and 41.05 ± 11.15, respectively, which was much higher than that determined by biodistribution (1.34 ± 0.09 and 7.42 ± 0.61; Fig. 5). This is probably because of the relatively high background activity in normal tissues due to *in vivo* deiodination, resulting in underestimated tumor uptake and *T/M* ratio in biodistribution studies. However, these values are parallel to the boron content in organs (Fig. 6).

An imaging-driven selection would help the physician to non-invasively identify patients who will benefit from BNCT. In the clinic,

prior to receiving the injection of BPA for BNCT, the patients need to undergo an ^{18}F-FBPA PET imaging to verify that the *T/M* ratio is approximately 3, to save time and money. We demonstrated that the tumor accumulation of ^{123}I-61-B-AuNPs in microSPECT images and biodistribution studies could reflect the boron content of the tumor (Fig. 6), suggesting that this imaging platform would predict the treatment outcome as well as BPA-based BNCT. Although our understanding of pharmacokinetics, cell-type dependence or variability, optimal 61 IgG coverage, and the real treatment response after neutron beam irradiation is incomplete, this is a proof-of-concept study showing the potential of radiolabeled, antibody-modified AuNPs as a theranostic assembly for BNCT.

5. Conclusion

Nowadays, patients who are planned to receive BNCT undergo ^{18}F-FBPA PET imaging prior to treatment for patient selection to determine the uptake of ^{18}F-FBPA in tumor and muscle. If the T/M ratio does not reach 3, a good tumor response cannot be guaranteed after BNCT. Therefore, in this study, we aimed to develop a potential boron-containing agent that can not only be specifically localized in the tumor but also be tracked using noninvasive imaging as well as ^{18}F-FBPA. In fact, many carborane- or boron cage-linked nanoparticles have been synthesized and their ability has been demonstrated in previous literature; however, none of these can be detected by noninvasive imaging for monitoring pharmacokinetics or predicting therapeutic efficacy. ^{123}I-61-B-AuNPs demonstrated high tumor accumulation in microPET imaging and biodistribution studies, and the boron content in tumor was confirmed by ICP-MS, showing the potential of antibody-modified boron-containing AuNPs as a boron drug for BNCT.

Acknowledgment

The authors thank the financial support from Ministry of Science and Technology, Taiwan (MOST 104-2314-B-039-030-MY3) and technical support from Medical Research Core Facility, Office of Research & Development at China Medical University, Taiwan, and Center for Advanced Molecular Imaging and Translation, Chang Gung Memorial Hospital, Taiwan.

Appendix A. Supplementary data

Supplementary material related to this article can be found, in the online version, at doi:https://doi.org/10.1016/j.colsurfb.2019.110387.

References

[1] R.F. Barth, P. Mi, W. Yang, Boron delivery agents for neutron capture therapy of cancer, Cancer Commun. (Lond.) 38 (2018) 35, https://doi.org/10.1186/s40880-018-0299-7.
[2] T. Kubota, S. Kuroda, N. Kanaya, T. Morihiro, K. Aoyama, Y. Kakiuchi, et al., HER2-targeted gold nanoparticles potentially overcome resistance to trastuzumab in gastric cancer, Nanomedicine 14 (2018) 1919–1929, https://doi.org/10.1016/j.nano.2018.05.019.
[3] W. Ratynski, F. Kappeler, Neutron-Capture Cross-Section of Au-197 — a Standard for Stellar Nucleosynthesis, Phys. Rev. C 37 (1988) 595–604, https://doi.org/10.1103/PhysRevC.37.595.
[4] N.S. Hosmane, Boron Science: New Technologies and Applications, CRC Press, 2016.
[5] N.S. Hosmane, R. Eagling, Handbook of Boron Science, World Scientific, 2019.
[6] N.S. Hosmane, J.A. Maguire, Y. Zhu, Boron and Gadolinium Neutron Capture Therapy for Cancer Treatment, World Scientific, 2012.
[7] R. Djeda, J. Ruiz, D. Astruc, R. Satapathy, B.P. Dash, N.S. Hosmane, "Click" synthesis and properties of carborane-appended large dendrimers, Inorg. Chem. 49 (2010) 10702–10709, https://doi.org/10.1021/ic101729s.
[8] L.Y. Liang, A. Rapakousiou, L. Salmon, J. Ruiz, D. Astruc, B.P. Dash, et al., "Click" assembly of carborane-appended polymers and stabilization of gold and palladium nanoparticles, Eur. J. Inorg. Chem. (2011) 3043–3049, https://doi.org/10.1002/ejic.201100360.
[9] N. Li, P. Zhao, L. Salmon, J. Ruiz, M. Zabawa, N.S. Hosmane, et al., "Click" star-shaped and dendritic PEGylated gold nanoparticle-carborane assemblies, Inorg. Chem. 52 (2013) 11146–11155, https://doi.org/10.1021/ic4013697.
[10] A.M. Cioran, F. Teixidor, Z. Krpetic, M. Brust, C. Vinas, Preparation and characterization of Au nanoparticles capped with mercaptocarboranyl clusters, Dalton Trans. 43 (2014) 5054–5061, https://doi.org/10.1039/c3dt52872c.
[11] F. Chen, K. Ma, B. Madajewski, L. Zhuang, L. Zhang, K. Rickert, et al., Ultrasmall targeted nanoparticles with engineered antibody fragments for imaging detection of HER2-overexpressing breast cancer, Nat. Commun. 9 (2018) 4141, https://doi.org/10.1038/s41467-018-06271-5.
[12] W.Y. Kuo, J.J. Lin, H.J. Hsu, H.S. Chen, A.S. Yang, C.Y. Wu, Noninvasive assessment of characteristics of novel anti-HER2 antibodies by molecular imaging in a human gastric cancer xenograft-bearing mouse model, Sci. Rep. 8 (2018) 13735, https://doi.org/10.1038/s41598-018-32094-x.
[13] H.W. Kao, Y.Y. Lin, C.C. Chen, K.H. Chi, D.C. Tien, C.C. Hsia, et al., Evaluation of EGFR-targeted radioimmuno-gold-nanoparticles as a theranostic agent in a tumor animal model, Bioorg. Med. Chem. Lett. 23 (2013) 3180–3185, https://doi.org/10.1016/j.bmcl.2013.04.002.
[14] S. Kumar, J. Aaron, K. Sokolov, Directional conjugation of antibodies to nanoparticles for synthesis of multiplexed optical contrast agents with both delivery and targeting moieties, Nat. Protoc. 3 (2008) 314–320, https://doi.org/10.1038/nprot.2008.1.
[15] T.A. Kean, Rheumatoid arthritis and gold salts therapy, Ulster Med. J. 3 (1934) 284–289.
[16] W. Jiang, B.Y. Kim, J.T. Rutka, W.C. Chan, Nanoparticle-mediated cellular response is size-dependent, Nat. Nanotechnol. 3 (2008) 145–150, https://doi.org/10.1038/nnano.2008.30.
[17] W.Y. Kuo, H.J. Hsu, C.Y. Wu, H.S. Chen, Y.C. Chou, Y.L. Tsou, et al., Antibody-drug conjugates with HER2-targeting antibodies from synthetic antibody libraries are highly potent against HER2-positive human gastric tumor in xenograft models, MAbs 11 (2019) 153–165, https://doi.org/10.1080/19420862.2018.1541370.
[18] H.S. Chen, S.C. Hou, J.W. Jian, K.S. Goh, S.T. Shen, Y.C. Lee, et al., Predominant structural configuration of natural antibody repertoires enables potent antibody responses against protein antigens, Sci. Rep. 5 (2015) 12411, https://doi.org/10.1038/srep12411.